RESEARCH ARTICLE

NANO · MICRO small
www.small-journal.com

Z-Scheme Heterojunction of Hierarchical $Cu_2S/CdIn_2S_4$ Hollow Cubes to Boost Photoelectrochemical Performance

*Si Zhang, Jiahui Sun, and Huangxian Ju**

The exaltation of light-harvesting efficiency and the inhibition of fast charge recombination are pivotal to the improvement of photoelectrochemical (PEC) performance. Herein, a direct Z-scheme heterojunction is designed of $Cu_2S/CdIn_2S_4$ by in situ growth of $CdIn_2S_4$ nanosheets on the surface of hollow CuS cubes and then annealing at 400 °C. The constructed Z-scheme heterojunction is demonstrated with electron paramagnetic resonance and redox couple (*p*-nitrophenol/*p*-aminophenol) measurements. Under illumination, it shows the photocurrent 6 times larger than that of hollow Cu_2S cubes, and affords outstanding PEC performance over the known Cu_2S and $CdIn_2S_4$-based photocatalysts. X-ray photoelectron spectroscopy and density functional theory results demonstrate a strong internal electric field formed in $Cu_2S/CdIn_2S_4$ Z-scheme heterojunction, which accelerates the Z-scheme charge migration, thereby promoting electron–hole separation and enhancing their utilization efficiency. Moreover, the hollow structure of Cu_2S is conducive to shortening the charge transport distance and improving light-harvesting capability. In proof-of-concept PEC application, a PEC detection method for miRNA-141 based on the sensitivity of benzo-4-chloro-hexadienone to light absorption on $Cu_2S/CdIn_2S_4$ modified electrode is developed with good selectivity and a limit of detection of 32 aM. This work provides a simple approach for designing photoactive materials with highly efficient PEC performance.

1. Introduction

Photoelectrochemistry (PEC) involves photon-to-electricity conversion, charge transfer, and electron exchange at the electrode/solution interface. It generally undergoes the acceptance of photon energy by the photoactive materials to generate electron–hole pairs under light irradiation, subsequent migrating of charge from the materials to the electrodes for electrical signal output, and the caused oxidation-reduction reaction occurring at the interface.[1–3] The photoelectric conversion efficiency is a key parameter determining PEC performance. But it is often unsatisfactory with the inefficient utilization of light and the rapid electron–hole recombination, thereby hindering its application.[4,5] Hence, it is of great significance to rational design and precisely fabricate photoactive materials to improve the PEC performance.

Recently, metal chalcogenide materials have gained enormous attention in many advanced applications including photocatalytic water splitting, photocatalytic H_2 generation, and PEC sensing due to their large compositional diversity and favorable visible light response.[6,7] Among these materials, Cu_2S has an adjustable narrow bandgap (1.2–2.1 eV), strong light absorption, and high conductivity, and has been proved to be a promising photoactive material.[8,9] Nevertheless, the pure Cu_2S also suffers from serious electron–hole recombination and slow charge-transfer kinetic, which severely limit the PEC activity of Cu_2S. To overcome these obstacles in improving photoelectric conversion efficiency, several strategies such as phase and morphology regulation, doping, cocatalysts deposition, defect engineering, and heterojunction constructing have been developed.[10–13] Among these strategies, the construction of heterojunction through coupling various materials with staggered bandgaps has become an effective protocol.[14] Especially, the direct Z-scheme heterojunction has attractive advantages in accelerating the electron–hole separation and charge transfer, broadening the light absorption range, and maintaining high redox capability.[15–17] Moreover, the internal electric field in the direct Z-scheme heterojunction, which is formed by asymmetric charge distribution, has been proved as a powerful driving force for triggering the separation of electrons and holes and promoting them to migrate in opposite directions.

Up to now, the developed Cu_2S-based heterojunctions mainly are type II. These heterojunctions can improve the separation efficiency of electron–hole pairs but greatly reduce the redox activity at the interface.[18] Therefore, incorporating a semiconductor and Cu_2S to form direct Z-scheme heterojunction is a meaningful and urgent need for further boosting the PEC performance of Cu_2S-based photoactive materials. In addition, morphology and structure regulation is also a feasible route to improve the PEC performance of photoactive materials. The hollow structure can shorten the travel path of the charge to the surface, and enhance light absorption and utilization, thus has attracted

S. Zhang, J. Sun, H. Ju
State Key Laboratory of Analytical Chemistry for Life Science
School of Chemistry and Chemical Engineering
Nanjing University
Nanjing 210023, P. R. China
E-mail: hxju@nju.edu.cn

The ORCID identification number(s) for the author(s) of this article can be found under https://doi.org/10.1002/smll.202405712

DOI: 10.1002/smll.202405712

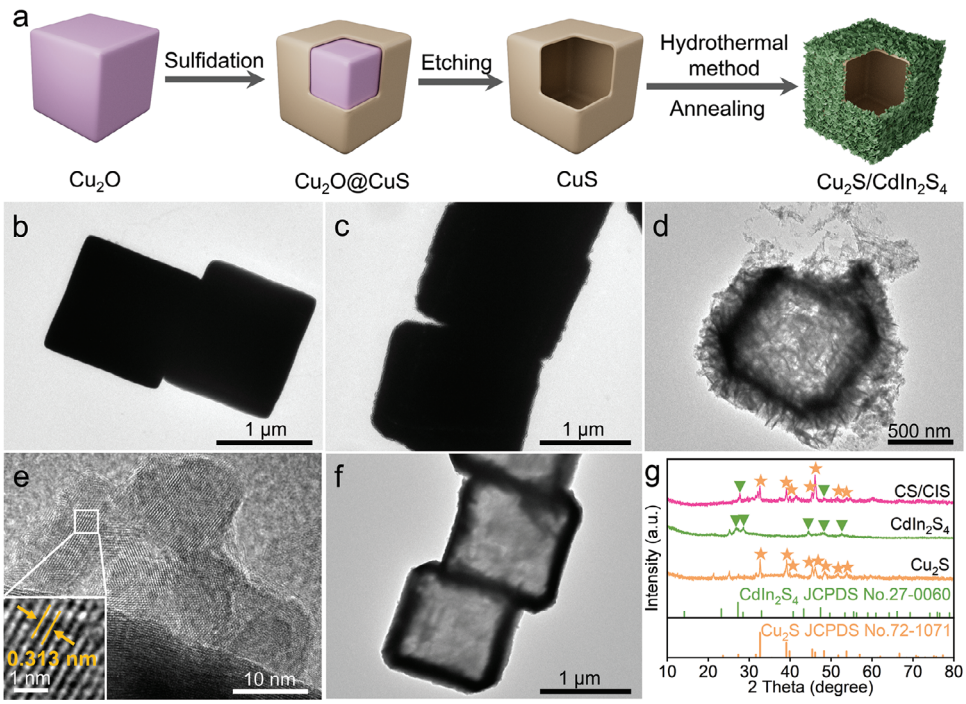

Figure 1. a) Schematic illustration of the synthesis process of CS/CIS. TEM images of b) Cu_2O cubes, c) Cu_2O@CuS cubes, and d) CS/CIS. e) HR-TEM image of CS/CIS. f) TEM image of hollow Cu_2S cubes. g) XRD patterns of hollow Cu_2S cubes, flower-like $CdIn_2S_4$, and CS/CIS.

numerous attention of researchers.[19] For example, the visible-light-responsive $Co_9S_8/ZnIn_2S_4$ with hierarchical hollow tubular structure and heterojunction has been prepared for enhancing visible-light H_2 evolution and reduction of aqueous Cr^{VI}.[20] In view of the appropriate bandgap,[21,22] superior thermal and structural constancy and easy availability of $CdIn_2S_4$, a typical ternary semiconductor material, this work in situ grows $CdIn_2S_4$ on the surface of hollow CuS cubes and then transforms the CuS to Cu_2S with an annealing process at 400 °C to construct for the first time a Z-scheme heterojunction of hierarchical $Cu_2S/CdIn_2S_4$ hollow cubes (CS/CIS) for achieving high PEC performance. Due to the well-matched staggered band alignment and work function difference between Cu_2S and $CdIn_2S_4$, this Z-scheme heterojunction shows a strong internal electric field, which promotes the separation of electron–hole pairs. Benefiting from the hollow structure of Cu_2S for enhancing charge transport and light utilization efficiency, the photocurrent increases by ≈10 times compared to snowflake-like Cu_2S. The Z-scheme heterojunction leads to a further increase of photocurrent by 6 times, affording outstanding PEC performance over the known Cu_2S and $CdIn_2S_4$-based photocatalysts. In proof-of-concept application of the excellent PEC performance, a PEC detection method for miRNA-141, a biomarker for early diagnosis and biotherapy of cancer,[23] is developed by drop-casting miRNA-141-related precipitates on CS/CIS modified electrode to suppress the light absorption. As the PEC immunoassay and aptasensor,[24] this method shows the advantages of fast response time, simple instrumentation, effective separation of excitation light source, and detection of current signal. This work provides a new avenue to improve the PEC performance of photoactive materials via rational design of Z-scheme heterojunction.

2. Results and Discussion

The hollow CuS cubes were first synthesized with home-made Cu_2O cubes as corrosion-prone templates by using Na_2S for sulfidation and $Na_2S_2O_3$ for etching (**Figure 1a**). Subsequently, the $CdIn_2S_4$ nanosheets were grown on the surface of hollow CuS cubes via the hydrothermal method to obtain $CuS/CdIn_2S_4$, which were finally annealed at 400 °C for 1 h in an argon atmosphere to trigger CuS decomposition for forming hierarchical $Cu_2S/CdIn_2S_4$ hollow cubes (CS/CIS). The home-made Cu_2O presented a uniform solid cube shape with a smooth surface (Figure 1b; Figure S1a, Supporting Information). Powder X-ray diffraction (XRD) pattern confirmed the successful preparation of Cu_2O cubes (Figure S2, Supporting Information). After sulfidation with Na_2S, the Cu_2O external shell on cubes was converted into CuS to form Cu_2O@CuS cubes,[25] which exhibited a slightly rough surface (Figure 1c; Figure S1b, Supporting Information). The etching of Cu_2O@CuS cubes with $Na_2S_2O_3$ led to the formation of hollow cube structure (Figure S3a, Supporting Information), which showed two XRD peaks attributed to hexagonal-phase CuS (JCPDS No.78-0876) along with an impurity peak for Cu_7S_4 (Figure S3b, Supporting Information),[25] proving a hollow CuS cube structure with a thickness of ≈90 nm (Figure 1d). The $CdIn_2S_4$ film grown on hollow Cu_2S cubes showed a thickness of ≈140 nm and a surface structure similar to the flower-like microsphere of $CdIn_2S_4$ prepared in the absence of hollow CuS cubes and annealing process (Figure 1d; Figures S1c–S4, Supporting Information). The high-resolution TEM (HR-TEM) image of CS/CIS (Figure 1e) demonstrated a spacing of lattice fringe with 0.313 nm, which was attributed to the (222) plane of $CdIn_2S_4$ on hollow Cu_2S cubes. To demonstrate the

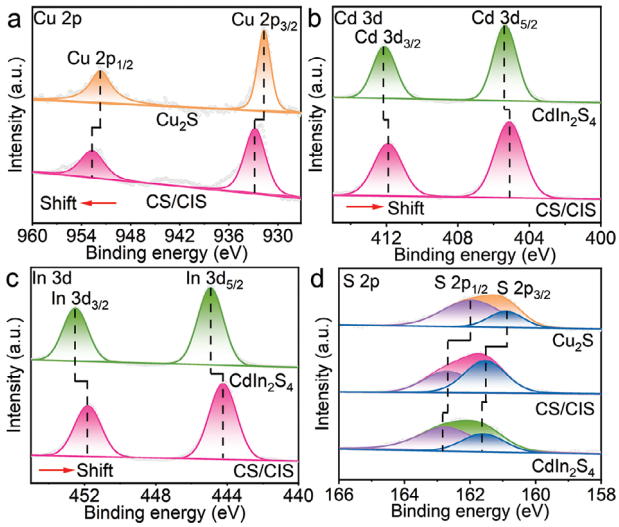

Figure 2. High-resolution XPS spectra of a) Cu 2p, b) Cd 3d, c) In 3d and d) S 2p for hollow Cu_2S cubes, flower-like $CdIn_2S_4$ and CS/CIS.

decomposition of CuS in CuS/$CdIn_2S_4$ to form CS/CIS via an annealing process, the synthesized CuS cubes were directly annealed at 400 °C for 1 h in an argon atmosphere, which also produced a hollow structure (Figure 1f; Figure S1d, Supporting Information). Interestingly, the sulfidation of Cu_2O cubes with Na_2S, the etching of Cu_2O@CuS cubes with $Na_2S_2O_3$, and the annealing treatment of hollow CuS cubes did not change the size of the cubes with a side length of ≈1 µm. Moreover, the CS/CIS showed uniform distribution of Cu, S, Cd, and In elements over the cubes (Figure S5, Supporting Information), and the characteristic diffraction peaks attributing to the tetragonal phase of Cu_2S (JCPDS No.72-1071) and the cubic phase of $CdIn_2S_4$ (JCPDS No.27-0060) in the XRD pattern (Figure 1g).[25–27] Those results demonstrated the successful preparation of CS/CIS and the tight adherence between grown $CdIn_2S_4$ and hollow Cu_2S cubes.

The X-ray photoelectron spectroscopy (XPS) was applied to explore the chemical composition and chemical states of CS/CIS. The XPS survey spectra confirmed the existence of Cu, Cd, In, and S elements in CS/CIS (Figure S6, Supporting Information), in according with the EDS results (Figure S5, Supporting Information). The high-resolution Cu 2p spectrum of CS/CIS showed two peaks at 952.7 and 932.8 eV, which were assigned to the binding energies of Cu $2p_{1/2}$ and Cu $2p_{3/2}$ for Cu^+, respectively (**Figure** 2a). The Auger Cu LMM XPS spectrum also demonstrated the presence of Cu^+ (Figure S7, Supporting Information).[9] Two characteristic peaks at 411.9 and 405.1 eV in Cd 3d spectrum of CS/CIS corresponded to Cd $3d_{3/2}$ and Cd $3d_{5/2}$ (Figure 2b), verifying the Cd^{2+} states.[28] The peaks in In 3d spectrum of CS/CIS located at 451.8 and 444.2 eV (Figure 2c), matching well with the characteristic peaks of In $3d_{3/2}$ and In $3d_{5/2}$ for In^{3+}, respectively.[29] Two peaks at 162.7 and 161.6 eV in S 2p spectrum of CS/CIS were assigned to S $2p_{1/2}$ and S $2p_{3/2}$ for S^{2-}, respectively (Figure 2d).[30] Compared to the characteristic peaks of hollow Cu_2S cubes and flower-like $CdIn_2S_4$, all the spectra of CS/CIS showed the shifts of element-binding energy, which could directly reflect the changes of electron density due to the tight adherence of $CdIn_2S_4$ on hollow Cu_2S cubes. It is worth noting that Cu^+ showed a positive shift after forming CS/CIS, while the adherence of $CdIn_2S_4$ led to negative shifts of both Cd^{2+} and In^{3+}, confirming the existence of vigorously interfacial interaction between hollow Cu_2S cubes and $CdIn_2S_4$ with the electron migration from hollow Cu_2S cubes to $CdIn_2S_4$.[31,32]

The optical properties and bandgaps of CS/CIS were investigated with the UV–vis diffuse reflectance spectra (UV–vis DRS). Hollow Cu_2S cubes presented intense light absorption in 200–800 nm (**Figure** 3a), suggesting its strong light-harvesting capability due to the narrow bandgap.[8,9] However, the light absorption of $CdIn_2S_4$ was limited in a region up to 530 nm. After covering $CdIn_2S_4$ on hollow Cu_2S cubes, the light-harvesting capability was enhanced, and the light absorption range was extended to ≈590 nm, which was attributed to the formation of heterojunction. The enhanced light absorption was beneficial to the separation of more electrons and holes, and thus the improvement of the PEC activity of CS/CIS. The optical bandgap energy (E_g) of hollow Cu_2S cubes and $CdIn_2S_4$ could be calculated from Tauc plots (Figure S8, Supporting Information) to be 1.59 and 2.42 eV, respectively.[33–35]

The band positions of the hollow Cu_2S cubes and $CdIn_2S_4$ were confirmed by Mott–Schottky (M–S) plot (Figure 3b,c). Clearly, the flat band potentials (E_{fb}) of Cu_2S cubes and $CdIn_2S_4$ were determined to be 0.41 and −0.54 V versus NHE (normal hydrogen electrode), respectively, by extending the linear part of M–S plots. The negative slope of M–S plot implied the p-type conductive property of Cu_2S cubes, while the M–S plot of $CdIn_2S_4$ with positive slope suggested an n-type semiconductor.[36] According to the previous report,[37] the conduction band potential (E_{CB}) of n-type semiconductor was ≈0.2 V negative than the E_{fb}, while the valence band potential (E_{VB}) of the p-type semiconductor was ≈0.2 V positive than the E_{fb}. Thus the E_{VB} of Cu_2S cubes and the E_{CB} of $CdIn_2S_4$ were determined to be 0.61 and −0.74 V (vs NHE), respectively. According to the equation of $E_{VB} = E_{CB} + E_g$, the E_{CB} of the Cu_2S cubes and the E_{VB} of $CdIn_2S_4$ were calculated as −0.98 and 1.68 V versus NHE, respectively. UV photoelectron spectroscopy (UPS) was also carried out to determine their electronic structural properties as well as E_{VB} and E_{CB} positions (Figure S9, Supporting Information).[38] Their band structures were in good accordance with those evaluated with M–S plots, as listed in Table S1 (Supporting Information). The energy level diagrams of hollow Cu_2S cubes and $CdIn_2S_4$ could be shown in Figure 3d, indicating their matched and staggered energy band alignments, which was favorable to the construction of Z-scheme heterojunction.

To better evaluate the charge separation properties of hollow Cu_2S cubes and CS/CIS, their steady-state photoluminescence (PL) and time-resolved PL (TRPL) spectra were measured. Generally, the PL peak is generated from the recombination of electron–hole, that is, lower intensity of PL peak indicates the efficient charge separation. The hollow Cu_2S cubes exhibited a prominent emission peak (Figure 3e), implying the rapid electron–hole recombination. The emission of CS/CIS was remarkably quenched, but showed a prolonged lifetime (2.87 ns) compared to 0.97 ns of hollow Cu_2S cubes (Figure S10, Table S2, Supporting Information), suggesting the greatly promoted charge separation and transfer efficiency in CS/CIS.

To verify the advantages of a hollow structure, Cu_2S particles were synthesized according to the previous report.[39] The

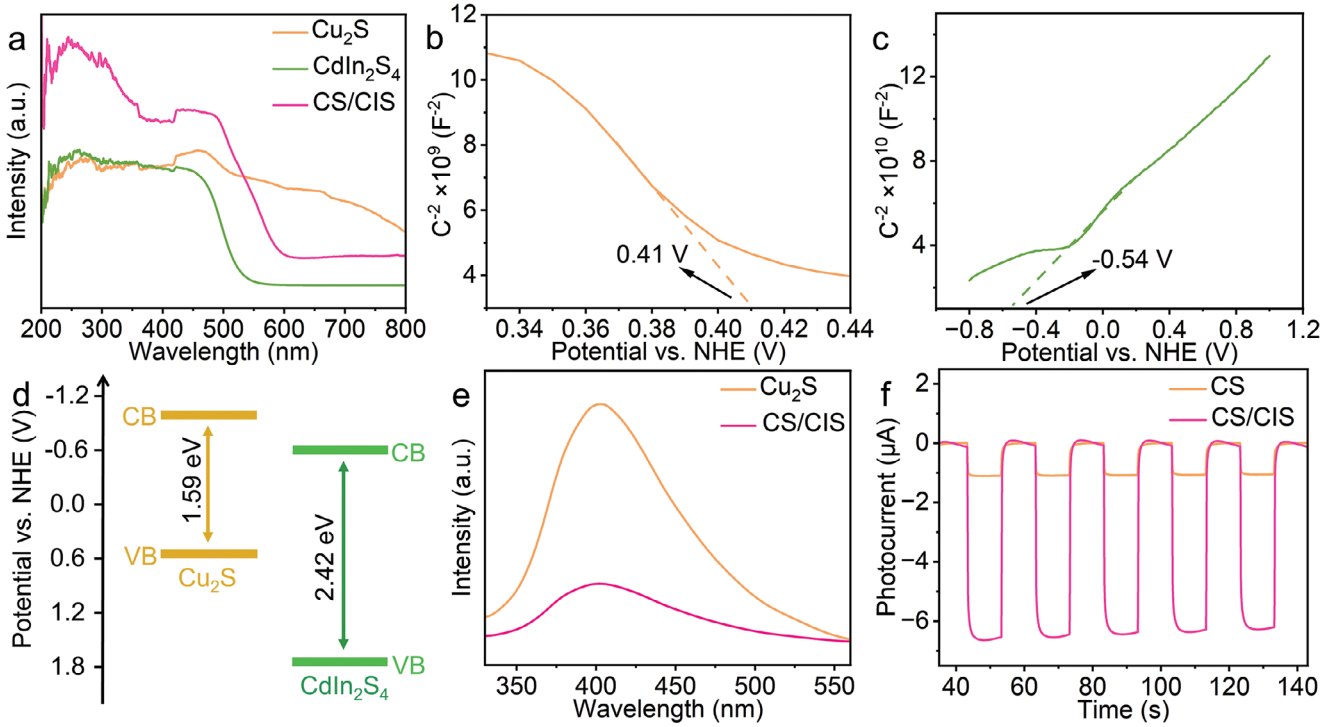

Figure 3. a) UV–vis DRS of hollow Cu_2S cubes and flower-like $CdIn_2S_4$, and CS/CIS. b–d) M-S plots of Cu_2S cubes and $CdIn_2S_4$, and their band structure alignments. e) PL spectra of Cu_2S cubes and CS/CIS. f) Transient photocurrent responses of hollow Cu_2S cubes modified ITO and CS/CIS/ITO in PBS (0.01 M, pH 7.0) containing 0.1 M NaCl at an applied potential of 0 V.

obtained Cu_2S particles showed a snowflake-like structure and the XRD pattern corresponding to the orthorhombic-phase of Cu_2S (JCPDS No.02-1294) (Figure S11a,b, Supporting Information). Compared to the snowflake-like Cu_2S, the hollow Cu_2S cubes modified electrode of indium tin oxides (ITO) showed 10 times larger photocurrent response (Figure S11c, Supporting Information). This could be attributed to the enhanced light utilization of the hollow structure by multiple light reflections inside the hollow Cu_2S cubes and the shortened charge transport distance, as shown in Figure S12 (Supporting Information), which caused more electrons and holes to be generated and accelerated charge transfer from Cu_2S to electrode. After growing $CdIn_2S_4$ on hollow Cu_2S cubes, the resulting CS/CIS/ITO showed 6 times higher photocurrent than the pristine Cu_2S cubes modified ITO (Figure 3f), indicating the better charge separation and migration properties in CS/CIS/ITO, which was demonstrated by the significantly increased incident photon-to-current conversion efficiency (IPCE) of CS/CIS/ITO under monochromatic light irradiation of 360–650 nm (Figure S13, Supporting Information). The electrochemical impedance spectra (EIS) of the modified ITOs further demonstrated the accelerated charge transfer from CS/CIS to electrode (Figure S14, Supporting Information). More importantly, the designed CS/CIS possessed the best PEC performance compared to the reported Cu_2S and $CdIn_2S_4$-base materials (Table S3, Supporting Information). In addition, after continuous irradiation for 1 h, the TEM image, XRD pattern and XPS spectra of CS/CIS did not obviously change (Figure S15, Supporting Information), indicating its good stability in morphology, structure, and components.

To validate the interfacial charge transfer mechanism between hollow Cu_2S cubes and $CdIn_2S_4$ layer, electron paramagnetic resonance (EPR) experiments were performed to determine the signal intensity of superoxide radical ($\bullet O_2^-$) and hydroxyl ($\bullet$OH) by using 5,5-dimethyl-1-pyrroline *N*-oxide (DMPO) as spin-trapping reagent.[40,41] After DMPO was mixed with flower-like $CdIn_2S_4$ or CS/CIS dispersion and irradiated under visible light for 2 min, no significant signal of DMPO-$\bullet$OH was observed (**Figure 4a**), which could be attributed to the fact that their E_{VB} values were too negative to oxidize $OH^-/\bullet OH$ (+1.99 V vs NHE).[42] On the contrary, the irradiated mixture of DMPO with flower-like $CdIn_2S_4$ showed weak DMPO-$\bullet O_2^-$ signal, and stronger DMPO-$\bullet O_2^-$ signal could be observed from the irradiated mixture of DMPO with hollow Cu_2S cubes (Figure 4b) owing to the more negative E_{CB} of Cu_2S cubes than the reduction potential of $O_2/\bullet O_2^-$ (−0.33 V vs NHE).[43] Notably, CS/CIS showed the strongest DMPO-$\bullet O_2^-$ signal, implying that the CS/CIS possessed a stronger reduction ability. In other words, more electrons were accumulated on the E_{CB} of hollow Cu_2S cubes of CS/CIS, different from type II heterojunction (Figure 4c), revealing that CS/CIS followed the Z-scheme charge transfer pathway in PEC process, and thus demonstrating the presence of Z-scheme heterojunction in CS/CIS.

The redox couple of *p*-nitrophenol (NP)/*p*-aminophenol (AP) was further used to support the Z-scheme charge transfer pathway in CS/CIS.[44] In the presence of hollow Cu_2S cubes and UV light irradiation, NP was reduced to AP via the electron transfer from the more negative CB of Cu_2S to NP with the reduction potential of −0.77 V versus NHE, resulting in a decreased

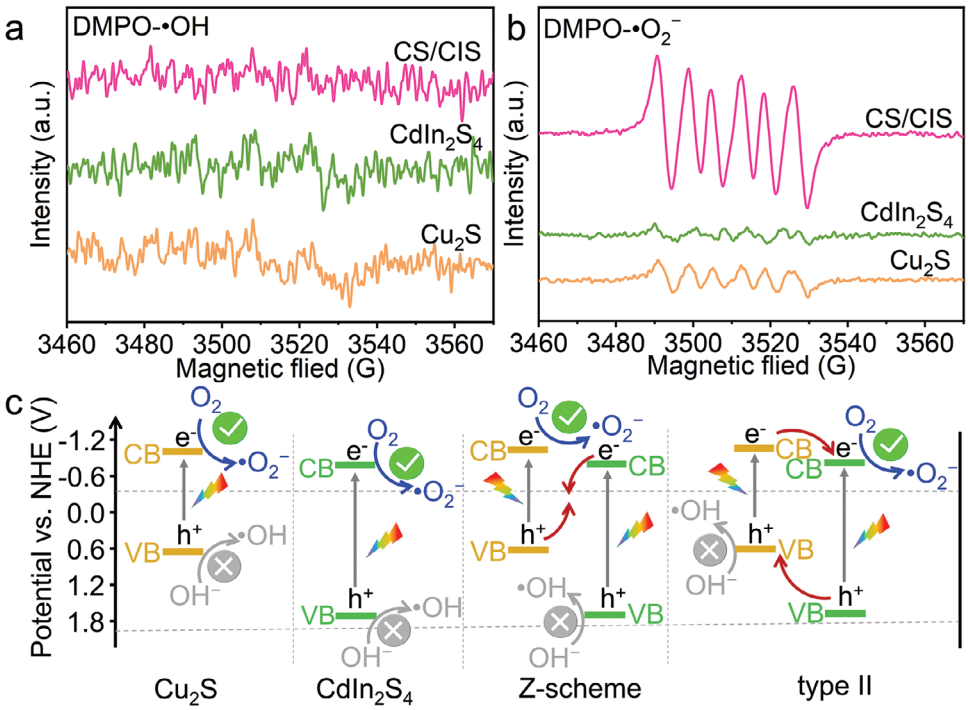

Figure 4. a,b) DMPO spin-trapping EPR spectra of hollow Cu_2S cubes, flower-like $CdIn_2S_4$ and CS/CIS in methanol for DMPO-•OH and in water for DMPO-•O_2^- under visible light irradiation ($\lambda \geq 420$ nm) for 2 min. c) Schematic illustration of charge transfer in Cu_2S cubes, $CdIn_2S_4$, Z-scheme heterojunction, and type II heterojunction.

absorbance (Figures S16 and S17, Supporting Information). However, the presence of $CdIn_2S_4$ did not change the absorbance intensity of NP, which could be attributed to the more positive E_{CB} of $CdIn_2S_4$ than the reduction potential of NP/AP. Obviously, CS/CIS also resulted in decreased absorbance, demonstrating the electron transfer. This unambiguously confirmed the direct Z-scheme heterojunction charge transfer pathway in CS/CIS.

Density functional theory (DFT) calculation was used to in-depth explore the interfacial charge transfer mechanism of CS/CIS. The work function (Φ) of hollow Cu_2S and $CdIn_2S_4$ was calculated with the electrostatic potential on the surfaces of Cu_2S (101) and $CdIn_2S_4$ (110) was 4.60 and 4.96 eV, respectively (**Figure** 5a,b). The Fermi level (E_F) of Cu_2S and $CdIn_2S_4$ was calculated to be 4.60 and 4.96 eV versus vacuum, respectively, which were 0.16 and 0.47 eV versus NHE.[45] Thus, the E_F of $CdIn_2S_4$ (110) was more positive than that of Cu_2S (101) (Figure 5c). Theoretically, the contact of Cu_2S (101) surface with $CdIn_2S_4$ (110) surface could result in spontaneous electron migration from Cu_2S to $CdIn_2S_4$ through the interface until an E_F equilibrium occurs. Due to the redistribution of charge at the interface of Cu_2S (101) and $CdIn_2S_4$ (110), the interface near Cu_2S (101) side became more positive, leading to upward bending of interface band edges due to the electron depletion for driving the electron transfer, while the interface near $CdIn_2S_4$ (110) became more negative and exhibited downward bending of interface band edge due to electron accumulation (Figure 5c). As a result, the uneven interfacial charge distribution resulted in the formation of an internal electric field pointing from Cu_2S to $CdIn_2S_4$, and thus generated a driving force for the separation of electrons and holes, which was consistent with the XPS results. Furthermore, the charge density difference between Cu_2S and $CdIn_2S_4$ at the interface also reflected the identical change of charge density (Figure 5d). Obviously, electron cloud density accumulates on S atoms of $CdIn_2S_4$, and depletes on Cu atoms of Cu_2S cubes.

In total, the charge transfer mechanism of CS/CIS under visible light irradiation could be elaborated in Figure 5c. The electrons on the valence band (VB) of Cu_2S and $CdIn_2S_4$ were first excited to their conduction band (CB), and the holes were left on the VB, respectively. Subsequently, the electrons on the CB of $CdIn_2S_4$ were driven by the internal electric field and band edge bending to migrate to the VB of Cu_2S to recombine with the holes in the interface. Thus, the electrons and holes were accumulated on the CB of Cu_2S and the VB of $CdIn_2S_4$, respectively, leading to enhanced oxidation and reduction ability. The Z-scheme heterojunction of CS/CIS not only accelerated the charge separation and transfer, but also retained the strong redox ability, thereby effectively improved the PEC performance. Besides, the hollow structure of Cu_2S was more favorable to enhancing light absorption and shortening the distance for the charge transfer from the interior to the surface (Figure S12, Supporting Information). All these advantages of Z-scheme heterojunction of CS/CIS greatly boost the PEC performance and are benefitting to the design of sensitive PEC detection methods.

To verify the application of the boosted PEC performance, a PEC detection method was developed with CS/CIS modified ITO electrode by taking miRNA-141 as an analyte model. As shown in Figure S18 (Supporting Information), after miRNA-141 was captured by magnetic bead-ssDNA (MB-ssDNA) to perform duplex specific nuclease (DSN)-assisted reaction at 50 °C for 90 min, which led to the release of output DNA from MB-ssDNA to

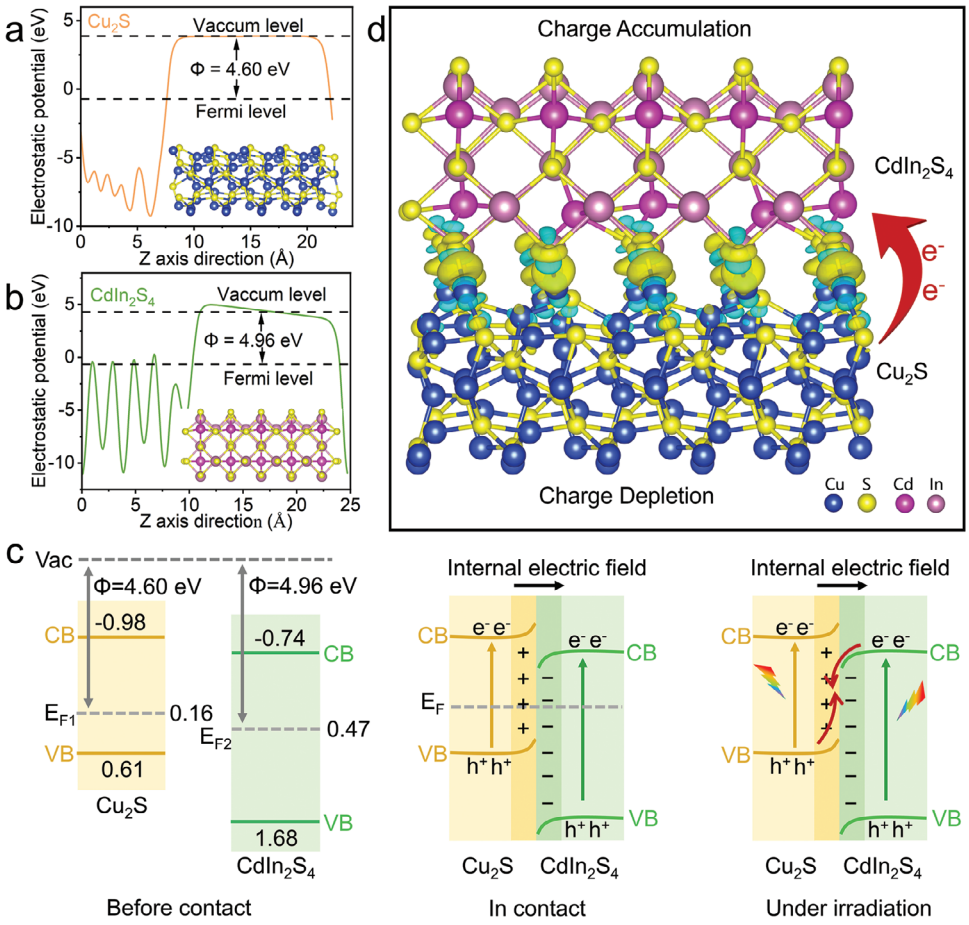

Figure 5. a,b) Work functions of Cu_2S and $CdIn_2S_4$. Insets: corresponding structural models. c) Schematic illustration of charge transfer of CS/CIS before contact, in contact, and under irradiation. d) Simulated electron density distribution at the interface of CS/CIS heterojunction. Yellow and cyan areas represent the depletion and accumulation of electrons.

activate the trans-cleavage activity of CRISPR-Cas12a system. The activated Cas12a was then mixed with the solution containing G-rich DNA (G-DNA) and hemin to inhibit the formation of G4-hemin DNAzyme via cleaving G-DNA. The amount of formed G4-hemin DNAzyme depended on the initial concentration of miRNA-141, and thus resulting in a miRNA-141-related detection signal by a G4-hemin DNAzyme-mediated catalytic reaction, which could be performed by the catalytic oxidation of 4-chloro-1-naphthol (4-CN) to generate benzo-4-chloro-hexadienone (4-CD) precipitates, and the inhibition of 4-CD drop-cast on CS/CIS/ITO on the PEC response.

The miRNA-141 triggered nonspecific cleavage ability of CRISPR-Cas12a system toward G-DNA and the generation of 4-CD precipitates was first verified by UV–vis absorption and diffuse reflectance spectra (Figures S19 and S20, Supporting Information). At the wavelength more than 400 nm, the added 4-CN did not affect the light absorption, while the produced 4-CD precipitates could compete with CS/CIS for light absorption, leading to miRNA-141-related photocurrent response and electron transfer resistance (Figure S21, Supporting Information) after drop-casting the produced 4-CD on CS/CIS/ITO, verifying the feasibility for PEC analysis of miRNA-141.

The PEC detection of miRNA-141 was performed with the CS/CIS prepared according to the optimal composition, and appropriate temperature and time for CRISPR/Cas12a digestion (Figure S22, Supporting Information) at an applied potential of 0 V. This proposed method showed a linear plot of photocurrent versus the logarithm of miRNA-141 concentration from 0.1 fM to 1 nM with a limit of detection of 32 aM (S/N = 3) (Figure S23, Supporting Information). Moreover, the photocurrent was stable during PEC measurements and storage of 4-CD drop-cast CS/CIS/ITO (Figure S24, Supporting Information). The CS/CIS/ITO electrodes showed excellent reproducibility with a relative standard deviation of 2.3% for photocurrent measurements at 5 electrodes prepared independently. The analytical performance was much better than many previous reports for miRNA-141 detection (Table S4, Supporting Information), indicating the advantages of the Z-scheme heterojunction.

The applicability of the proposed PEC method for miRNA-141 detection was validated with the cell lysates from MDA-MB-231 and HeLa cells (Figure S25, Supporting Information), which indicated high expression of miRNA-141 in MDA-MB-231 cells and low expression of miRNA-141 in the HeLa cells, consistent with those reported previously.[46,47]

3. Conclusion

This work designs a Z-scheme heterojunction to boost the PEC performance of Cu_2S-based photoactive materials by in situ growing $CdIn_2S_4$ on the surface of hollow CuS cubes followed by an annealing process to transform the CuS to Cu_2S. The $CdIn_2S_4$ shows a surface structure similar to the flower-like microsphere and can be tightly adhered to hollow Cu_2S cubes, which results in the shifts of element-binding energy and the electron migration from hollow Cu_2S cubes to $CdIn_2S_4$. The synthesized CS/CIS shows enhanced light absorption capability, accelerated electron–hole separation and charge transfer, and strengthened redox ability due to the presence of Z-scheme heterojunction, which has been demonstrated by its charge transfer pathway in PEC process and density functional theory (DFT) calculation, and leads to an internal electric field from Cu_2S cubes to $CdIn_2S_4$ and the photocurrent increase by 6 times. The hollow structure of Cu_2S is also favorable to enhancing light absorption and shortening the charge transfer distance for increasing the photocurrent ≈10 times. The developed CS/CIS possesses outstanding PEC performance over the known Cu_2S and $CdIn_2S_4$-based photocatalysts. A PEC detection method for miRNA-141 has also been developed to verify the application of the boosted PEC performance. This work provides a promising strategy to design high-performance heterojunction nanomaterials.

Supporting Information

Supporting Information is available from the Wiley Online Library or from the author.

Acknowledgements

This work was financially supported by the National Natural Science Foundation of China (21827812 and 21890741), and the Science and Technology Project of Nanjing City (202110023).

Conflict of Interest

The authors declare no conflict of interest.

Data Availability Statement

The data that support the findings of this study are available from the corresponding author upon reasonable request.

Keywords

$Cu_2S/CdIn_2S_4$ hollow cubes, hollow Cu_2S cubes, photocatalysts, photoelectrochemistry, Z-scheme heterojunction

Received: July 9, 2024
Revised: August 10, 2024
Published online:

[1] W.-W. Zhao, J.-J. Xu, H.-Y. Chen, *Chem. Soc. Rev.* **2015**, *44*, 729.
[2] J. Shu, D. Tang, *Anal. Chem.* **2020**, *92*, 363.
[3] W.-W. Zhao, J.-J. Xu, H.-Y. Chen, *Chem. Rev.* **2014**, *114*, 7421.
[4] X. Zhu, Y. Jia, Y. Liu, J. Xu, H. He, S. Wang, Y. Shao, Y. Zhai, Y. Zhu, *Angew. Chem., Int. Ed.* **2024**, *63*, 202405962.
[5] J. Ran, H. Zhang, S. Fu, M. Jaroniec, J. Shan, B. Xia, Y. Qu, J. Qu, S. Chen, L. Song, J. M. Cairney, L. Jing, S.-Z. Qiao, *Nat. Commun.* **2022**, *13*, 4600.
[6] X. Xin, Y. Li, Y. Zhang, Y. Wang, X. Chi, Y. Wei, C. Diao, J. Su, R. Wang, P. Guo, J. Yu, J. Zhang, A. J. Sobrido, M.-M. Titirici, X. Li, *Nat. Commun.* **2024**, *15*, 337.
[7] R. Li, H. Li, X. Zhang, B. Liu, B. Wu, B. Zhu, J. Yu, G. Liu, L. Zheng, Q. Zeng, *Adv. Funct. Mater.* **2024**, *34*, 2402797.
[8] Y. Wang, M. Liu, C. Wu, J. Gao, M. Li, Z. Xing, Z. Li, W. Zhou, *Small* **2022**, *18*, 2202544.
[9] Y. Zhang, Y. Huang, S. S. Zhu, Y. Y. Liu, X. Zhang, J. J. Wang, A. Braun, *Small* **2021**, *17*, 2100320.
[10] G. Ren, J. Zhao, Z. Zhao, Z. Li, L. Wang, Z. Zhang, C. Li, X. Meng, *Angew. Chem., Int. Ed.* **2023**, *63*, 202314408.
[11] S. Qin, N. Denisov, H. Kim, P. Schmuki, *Angew. Chem., Int. Ed.* **2024**, *63*, 202316660.
[12] H. Li, J. Zhang, X. Deng, Y. Wang, G. Meng, R. Liu, J. Huang, M. Tu, C. Xu, Y. Peng, B. Wang, Y. Hou, *Angew. Chem., Int. Ed.* **2023**, *63*, 202316384.
[13] H. Peng, H. Yang, J. Han, X. Liu, D. Su, T. Yang, S. Liu, C.-W. Pao, Z. Hu, Q. Zhang, Y. Xu, H. Geng, X. Huang, *J. Am. Chem. Soc.* **2023**, *145*, 27757.
[14] H. Zhang, Y. Gao, S. Meng, Z. Wang, P. Wang, Z. Wang, C. Qiu, S. Chen, B. Weng, Y. M. Zheng, *Adv. Sci.* **2024**, *11*, 2400099.
[15] X. Xu, L. Meng, J. Zhang, S. Yang, C. Sun, H. Li, J. Li, Y. Zhu, *Angew. Chem., Int. Ed.* **2023**, *63*, 202308597.
[16] Y. Zhu, J. Ren, G. Huang, C. L. Dong, Y. C. Huang, P. Lu, H. Tang, Y. Liu, S. Shen, D. Yang, *Adv. Funct. Mater.* **2024**, *34*, 2311623.
[17] R. Shen, G. Liang, L. Hao, P. Zhang, X. Li, *Adv. Mater.* **2023**, *35*, 2303649.
[18] L. Li, X. Dai, D. L. Chen, Y. Zeng, Y. Hu, X. W. Lou, *Angew. Chem., Int. Ed.* **2022**, *61*, 202205839.
[19] J. Pan, D. Wang, D. Wu, J. Cao, X. Fang, C. Zhao, Z. Zeng, B. Zhang, D. Liu, S. Liu, G. Liu, S. Jiao, Z. Xu, L. Zhao, J. Wang, *Adv. Sci.* **2024**, *11*, 2309293.
[20] S. Wang, B. Y. Guan, X. Wang, X. W. D. Lou, *J. Am. Chem. Soc.* **2018**, *140*, 15145.
[21] M. A. Mahadadalkar, S. W. Gosavi, B. B. Kale, *J. Mater. Chem. A* **2018**, *6*, 16064.
[22] T. Wang, Y. Chai, D. Ma, W. Chen, W. Zheng, S. Huang, *Nano Res.* **2017**, *10*, 2699.
[23] C. Huang, L. Zhang, Y. Zhu, Z. Zhang, Y. Liu, C. Liu, S. Ge, J. Yu, *Anal. Chem.* **2022**, *94*, 8075.
[24] W. Geng, G. Jiang, H. Liu, L. Xue, L. Ding, Y. Li, Y. Wu, R. Yang, *Small* **2023**, *19*, 2302829.
[25] Y. Fang, D. Luan, Y. Chen, S. Gao, X. W. Lou, *Angew. Chem., Int. Ed.* **2020**, *59*, 7178.
[26] C. Ling, X. Ye, J. Zhang, J. Zhang, S. Zhang, S. Meng, X. Fu, S. Chen, *Sci. Rep.* **2017**, *7*, 27.
[27] C. Xue, H. An, X. Yan, J. Li, B. Yang, J. Wei, G. Yang, *Nano Energy* **2017**, *39*, 513.
[28] R. Bariki, D. Majhi, K. Das, A. Behera, B. G. Mishra, *Appl. Catal., B* **2020**, *270*, 118882.
[29] L. Meng, M. Wang, H. Sun, W. Tian, C. Xiao, S. Wu, F. Cao, L. Li, *Adv. Mater.* **2020**, *32*, 2002893.
[30] J.-J. Wei, H.-B. Li, G.-Q. Wang, J.-Y. Zheng, A.-J. Wang, L.-P. Mei, T. Zhao, J.-J. Feng, *Anal. Chem.* **2022**, *94*, 12240.
[31] C. Q. Li, X. Du, S. Jiang, Y. Liu, Z. L. Niu, Z. Y. Liu, S. S. Yi, X. Z. Yue, *Adv. Sci.* **2022**, *9*, 2201773.
[32] Z. Zhu, H. Huang, L. Liu, F. Chen, N. Tian, Y. Zhang, H. Yu, *Angew. Chem., Int. Ed.* **2022**, *61*, 202203519.

[33] Y. W. Han, L. Ye, T. J. Gong, Y. Fu, *Angew. Chem., Int. Ed.* **2023**, *62*, 202306305.
[34] C. Cui, X. Zhao, X. Su, N. Xi, X. Wang, X. Yu, X. L. Zhang, H. Liu, Y. Sang, *Adv. Funct. Mater.* **2022**, *32*, 2208962.
[35] L. Meng, J. He, X. Zhou, K. Deng, W. Xu, P. Kidkhunthod, R. Long, Y. Tang, L. Li, *Nat. Commun.* **2021**, *12*, 5247.
[36] X. Wang, X. Wang, J. Huang, S. Li, A. Meng, Z. Li, *Nat. Commun.* **2021**, *12*, 4112.
[37] J. Zheng, Z. Lei, *Appl. Catal., B* **2018**, *237*, 1.
[38] H. S. Moon, K. C. Hsiao, M. C. Wu, Y. Yun, Y. J. Hsu, K. Yong, *Adv. Mater.* **2022**, *35*, 2200172.
[39] X. Zhang, Y. Guo, J. Tian, B. Sun, Z. Liang, X. Xu, H. Cui, *Appl. Catal., B* **2018**, *232*, 355.
[40] Z. Chen, J. Wang, M. Hao, Y. Xie, X. Liu, H. Yang, G. I. N. Waterhouse, X. Wang, S. Ma, *Nat. Commun.* **2023**, *14*, 1106.
[41] H. Zhang, S. Liu, A. Zheng, P. Wang, Z. Zheng, Z. Wang, H. Cheng, Y. Dai, B. Huang, Y. Liu, *Angew. Chem., Int. Ed.* **2024**, *63*, 202400965.
[42] W. Xu, W. Tian, L. Meng, F. Cao, L. Li, *Adv. Energy Mater.* **2021**, *11*, 2003500.
[43] J. Bian, Z. Zhang, J. Feng, M. Thangamuthu, F. Yang, L. Sun, Z. Li, Y. Qu, D. Tang, Z. Lin, F. Bai, J. Tang, L. Jing, *Angew. Chem., Int. Ed.* **2021**, *60*, 20906.
[44] D. Zhao, Y. Wang, C.-L. Dong, Y.-C. Huang, J. Chen, F. Xue, S. Shen, L. Guo, *Nat. Energy* **2021**, *6*, 388.
[45] L. Shi, D. Benetti, Q. Wei, F. Rosei, *Small* **2023**, *19*, 2300606.
[46] H. Yang, M. Hu, Z. Li, P. Zhao, L. Xie, X. Song, J. Yu, *Anal. Chem.* **2019**, *91*, 14577.
[47] Y.-N. Zheng, W.-B. Liang, C.-Y. Xiong, Y. Zhuo, Y.-Q. Chai, R. Yuan, *Anal. Chem.* **2017**, *89*, 9445.